1828
AKADÉMIAI KIADÓ
UNIVERSITY of DEBRECEN
International Review of Applied Sciences and Engineering
DOI:
10.1556/1848.2025.00941

ORIGINAL RESEARCH PAPER

Sustainable composite materials for UAVs: An analysis of *Morinda citrifolia* and *Tamarindus indica* bio-fibres

M. Vinothkumar[1], B. Kirubadurai[1]*, R. Jaganraj[1], G. Jegadeeswari[2], R. Pugazhenthi[3] and G. Manikandan[4]

[1] Vel Tech Rangarajan Dr. Sagunthala R&D Institute of Science and Technology, Chennai, India
[2] Saveetha Engineering College, Chennai, India
[3] Vels Institute of Science, Technology & Advanced Studies, Chennai, India
[4] Sri Rangapoopathi College of Engineering, Tamil Nadu, India

Received: October 30, 2024 • Accepted: March 17, 2025

ABSTRACT

Nowadays, aligned with the national mission, the growth of Unmanned Aerial Vehicle (UAV) application is enormous. This research work investigates the probability of adding epoxy resin with novel biofibres such as *Tamarindus indica* and *Morinda citrifolia* to fabricate a composite material. A sustainable outcome is delivered by adopting *Tamarindus indica* and *Morinda citrifolia* fibres in UAV frame materials, which combine increased mechanical strength and durability with good environmental conditions. Based on the mechanical test outcomes, the *Tamarindus indica* composite (ETI) indicates significant compressive strength with an optimum load-carrying capacity of 5.98 kN and notable tensile strength is a maximum of 8.13 MPa, therefore *Tamarindus indica* composite plate can be used in rigid or definite-shaped applications due to its high resistance to deformation. The *Morinda citrifolia* composite (ETC) indicated high flexibility rate due to carrying a flexural load (0.15 KN), so it can be used as a dampening or cushioning material to absorb the vibrational energy. These two novel biodegradable composite materials possess a lower density and a higher strength-to-weight ratio, which are important properties for decreasing power consumption and improving the UAV's endurance. We investigated the chemical and morphological characteristics of the novel composites using scanning electron microscopy (SEM) and Fourier-transform infrared spectroscopy (FTIR). These novel biomaterials significantly reduce vibrations from UAV propellers and metal corrosion. Based on the research outcomes, using novel bio composites increases the mechanical strength and lifespan of UAVs and it also reduces their weight and power consumption.

KEYWORDS

Unmanned Aerial Vehicles (UAVs), *Morinda citrifolia*, *Tamarindus indica*, power consumption, structural integrity

1. INTRODUCTION

In unmanned aerial vehicle industries, to achieve optimum performance, low-weight, high-strength, and highly durable materials are used for maximum performance. Conventionally, artificial fibre composites such as carbon and glass fibres have been utilized, but their major issue is high economic cost and non-biodegradability. Natural fibre composites obtained from renewable sources deliver a sustainable option due to their low weight, biodegradability, and low cost. The major concerns like mechanical performance, moisture sensitivity and fibre-matrix adhesion require further research study.

1.1. Knowledge gap & novelty statement

The development of biocomposite materials has increased significant attention due to growing environmental problems. The bio-fibre-based material for Fused Deposition Modelling (FDM)

*Corresponding author.
E-mail: bkirubadurai@gmail.com

AKJournals

emphasizes the benefits of bio-based feedstock in additive manufacturing and achieves biodegradability as well as decreases carbon footprint [1]. The overall characteristics of bast fibre-reinforced composites were analyzed, such as classification, mechanical behaviour, and automotive and construction applications [2]. Biofibre composite is an environmentally friendly alternative to conventional plastics in the food industry due to the sustainable nature and mechanical behaviour [3]. Thermoplastic composites reinforced with eco-friendly benign biofibres have shown enhanced fibre–matrix interaction and durability [4]. The biomechanical contributions of wood hemicelluloses to cellulose fibrillar networks have been investigated, giving valuable information into the structural role of matrix polysaccharides in biofibre composites [5]. High-performance biofibre composites using mat and unidirectional flax fibre reinforcements elaborated improved mechanical properties due to surface fibrillation, which enhances fibre–matrix bonding [6]. An idea of hybridizing biofibres for polymer composite enhancement has been shown to improve mechanical properties by strategic fibre blending [7]. In additive manufacturing, biofibre-based 3D printing has been investigated, focusing on printability challenges and the mechanical integrity of biofilament material [8]. The usage of natural-based pine cone residues in ABS composites for 3D printing has led to enhanced thermal and microstructural stability [9]. Studies on epoxy reinforced with surface-treated pineapple fibers, B_4C particles, and CTBN rubber composites show improved tensile, impact, and thermal properties, along with lower water absorption [10]. Further analysis confirmed enhancements in fatigue resistance, fracture toughness, and dynamic mechanical behaviour, showing better energy dissipation and long-span durability [11]. Additionally, mechanical and microscopic investigation of biocomposites made from *Tinospora cordifolia* and *Tectona grandis* conducted research into underutilized biofibres with potential for low-cost composite applications [12].

Existing works have extensively investigated bio-fibre composites like jute, hemp and flax in structural uses in the automobile and construction industries. However, the potential of *Tamarindus indica* and *Morinda citrifolia* as UAV structural materials like frames remains largely underexplored. Previous works have mainly concentrated on basic mechanical behaviours of bio composites, but few researchers have focussed on critical aspects like damping characteristics and acoustic behaviour in aerospace industry. This research additionally provides the comprehensive mechanical behaviour of *Tamarindus indica* and *Morinda citrifolia* bio composites and targeting their structural execution in UAV industries. The numerical investigation is carried out to validate the experimental outcomes of mechanical characteristics. This research delivers new knowledge into producing and facilitating bio composites for sustainable replacement of traditional UAV structures.

1.2. Objective and importance of the current research

This research evaluates the mechanical behaviours and structural analysis of bio composites for UAV structural frames, associated with the existing research gap. The novelty of this research is listed below:

- Comparative analysis of natural fibre composites for UAV structural frame.
- Evaluation of fibre treatments to improve mechanical characteristics and durability.
- Evaluating the adaptability of bio-fibre composites in decreasing UAV weight while keeping mechanical integrity.

By accommodating sustainable materials into the UAV frame, this research participates in the advancement of environmentally friendly aerospace composites, boosting lightweight design, decreasing carbon footprint, and improving mechanical performance.

2. MATERIALS AND METHODS

This research utilizes VBR 8912 as a thermoset epoxy matrix (bisphenol-A) having a molecular load of 195 g mol^{-1} and a kinetic viscous value of 12,000 cps. Vasavibala Resins Pvt. Ltd. of India supplied the curing agent (VBR 1209) that was used to dry the matrix. Natural fibres from the plants *Morinda citrifolia*, *Ipomoea staphylina*, *Tamarindus indica* and *Tinospora cordifolia* are sourced by Go Green Industrial Fibre India Pvt. Ltd. Fig. 1(a)–(d) shows the *Morinda citrifolia* trees, *Tamarindus indica* tree, *Tinospora cordifolia* shrubs and *Ipomoea staphylina* shrub, after the fibres were extracted.

- Tree Fibre from *Morinda citrifolia*: The tree fibre comes from the tropical small evergreen tree *Morinda citrifolia*, which is also known as noni. The fibres derived from this tree are commonly used in traditional weaving and textile manufacture due to their strength and durability. They can be processed and spun into threads for a multitude of uses.
- Fibre from the Tamarindus Indica Tree: *Tamarindus indica* is a leguminous tree which provides highly durable natural fibres, due to its higher tensile durability and flexibility.
- Shrub Fibre: *Tinospora cordifolia* is a tropical climbing shrub that goes by the names guduchi and heart-shaped leaves moonseed. Its leaves are crushed and used as particulates.
- Ipomoea Staphylina Shrub Fibre: *Ipomoea staphylina* is a tropical and subtropical plant that comes under the glory family. It can be combined with different fibres to enhance their qualities and strength.

Because they are renewable and have fewer environmental effects than synthetic fibres, these natural fibres are being investigated for their potential in a variety of applications. Their mechanical qualities include durability, flexibility and tensile strength, equipping them for a variety of conventional and industrial applications.

2.1. Preparation of the samples

The basic parameter of sample preparation is derived from existing research work [12]. The bio composite structure is

Fig. 1. (a) Sample of Morinda-citrifolia, (b) sample of Tamarindus–indica, (c) sample of *Tinospora cordifolia* shrub and (d) sample of *Ipomoea staphylina* shrub

made up of hand layup method and then inspected for ocular imperfections. The metal moulds are fabricated with appropriate size. The mould is initially purified for removing impurities. Further, the wax polish is applied on the mould to ensure easy detachment of composite. The epoxy resin with hardener is uniformly applied on the prepared mould later natural fibres are dispersed over the epoxy resin matrix. Further, the matrix is applied to arrest the displacement of fibre. Then 50 kg load is applied to define the shape and remove the voids present in the composite. Further the setup is cured in room temperature up to 5–6 h. Finally, the composite is removed from the mould by an ejector.

Figure 2 displays composite panels made from different natural fibres embedded in an epoxy matrix. The process of making these composite panels begins with the preparation of natural fibres such as *Morinda citrifolia*, *Tamarindus indica*, *Tinospora cordifolia* and *Ipomoea staphylina*. In order to guarantee homogeneous distribution inside the composite, these fibres are gathered, cleaned, dried and cut into uniform pieces. An epoxy resin is made by combining the resin and hardener in the right proportions. This resin was selected for its outstanding mechanical qualities and strong adherence to natural fibres. After that, the produced fibres are combined with the epoxy resin to form a homogeneous mixture that guarantees the fibres are distributed evenly. This slurry is placed into moulds made to guarantee that the fibres are aligned and compacted properly. To enable the epoxy to solidify and bind the fibres together, the mixture is either heated to hasten the curing process or let to cure at room temperature. In order to guarantee full epoxy resin polymerization, the composite panels may go through extra post-curing procedures after being taken out of the moulds during the initial curing period. The composite panels are then polished and trimmed to the correct size and surface quality. For each test per sample, it is fabricated as per specific ASTM standards. The boundary condition and specification are discussed in Table 1.

3. RESULT AND DISCUSSION

3.1. Mechanical characterization of bio composite

Tensile and flexural tests are carried out in EMC, ETI, ETC, and EIS bio composites by adhering to ASTM-D 695 and ASTM-D 790 standards. A universal testing machine with a specification of 2.1 mm s^{-1} transverse speed and 40 tons load is used to conduct tensile test. Similarly, for a compression test adhering to ASTM D 3039 and ASTM-D 2240 standards is used for microhardness test by durometer.

The above Table 2 presents the mechanical properties of four natural fibre composites derived from different plant sources, identified as EMC (*Morinda citrifolia*), ETI (*Tamarindus indica*), ETC (*Tinospora cordifolia*) and EIS (*Ipomoea staphylina*). The properties measured include tensile strength, flexural load, compression load and hardness (Shore D°). ETI exhibits the highest tensile strength at 8.13 MPa and the highest compression load at 5.98 KN indicating superior mechanical performance in both tension and compression. In contrast, ETC shows the highest hardness value of 59 Shore D° but has the lowest tensile strength (1.23 MPa) and flexural load (0.13 KN) suggesting it is hard but not very strong in tension or bending. With EMC exhibiting a tensile strength of 5.78 MPa, a flexural

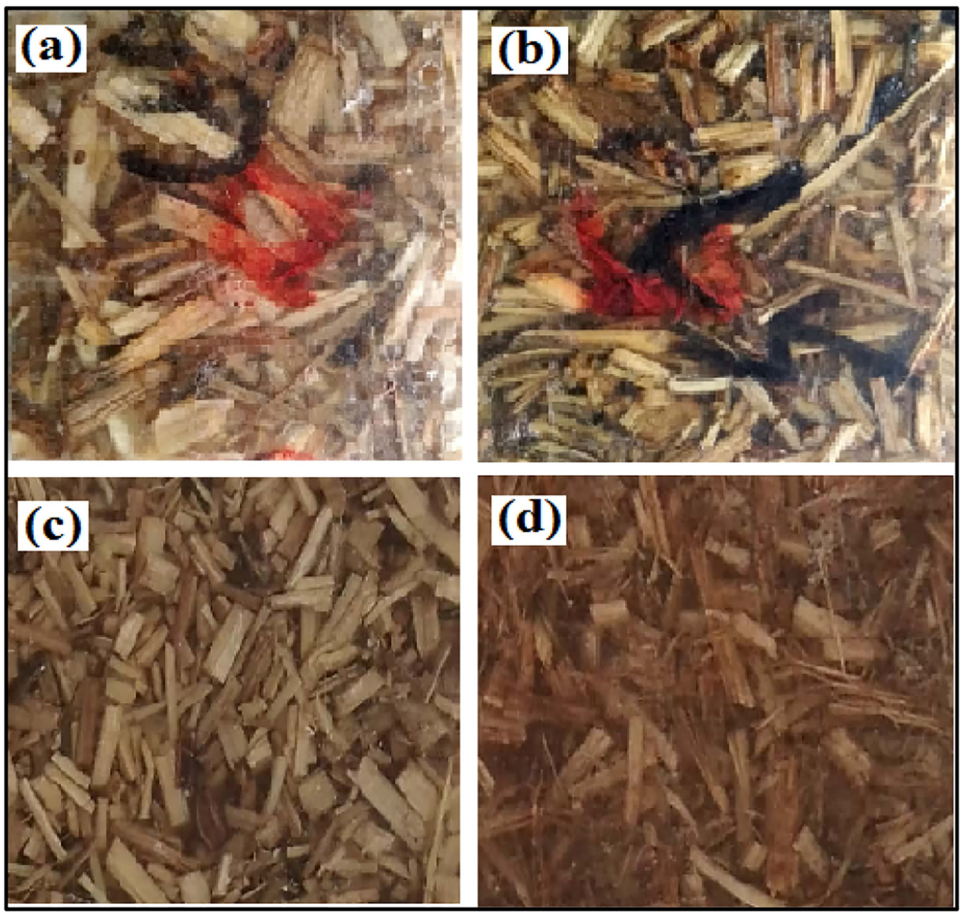

Fig. 2. (a) Epoxy morinda-citrifolia composite (EMC), (b) Epoxy tamarindus–indica composite (ETI), (c) Epoxy tinospora cordifolia composite (ETC) and (d) Epoxy *Ipomoea staphylina* composite (EIS)

load of 0.15 kN, a compression load of 1.92 KN and a hardness of 46 Shore D°, both EMC and EIS have reasonable values across all characteristics. EIS has the following properties: 45 Shore D° hardness, 2.78 MPa tensile strength, 0.19 KN flexural loads and 1.32 KN compression load. Based on the results, ETC is the suitable material where hardness is critical; in other cases, ETI is used for specific applications requiring intense tensile and compressive strength.

Figure 3 shows the EMC has a medium tensile strength in the 5 MPa range. ETI shows more tensile strength, near 8 MPa. In other cases, ETC exhibits a specified fall in tensile strength, around 2 MPa. EIS has a tensile strength of 3 MPa showing a small rise from ETC but still lower than EMC and ETI. From these analyses, ETI provides more strength among the other materials and ETC is considered a very weak material.

In Fig. 4, EMC possesses a flexural load of roughly 0.18 kN, ETI exhibits the maximum flexural load, topping near 0.32 kN. ETC exhibits a specific fall in flexural load around 0.12 kN, EIS increases slightly from ETC to around 0.2 kN. In Fig. 5, EMC indicates a compression load of about 2 kN. In this ETI, it exhibits the maximum value, topping near 6 kN. ETC shows a fall around 4 kN, but EIS indicates a lower range of about 1 kN. These two plot results suggest that ETI has superior strength due to its maximum flexural and compression loads compared with the other four. At the same time, in contrast, EIS possesses very weak strength when compared to the other four materials.

Figure 6 shows that EMC, ETI, ETC, and EIS exhibit the hardness range of 48 Shore D°, 55 Shore D°, 60 Shore D°, and 45 Shore D°, respectively. From these results, among four materials, ETC possesses a higher hardness value because of its hardness characteristics and the EIS exhibits the lower hardness value due to its softening nature.

Table 3 shows the mechanical properties of bio composites. From all the samples, Tamarindus exhibits the optimum tensile (8.13 MPa), flexural (32 MPa) and compressive strength (5.98 MPa), and shows higher mechanical execution.

Figure 7(a)–(c) indicates the stress-strain behaviour of four composite materials: EMC, ETI, ETC, and EIS.

- The Fig. 7(a) shows the tensile stress-strain curve, where ETI has the highest tensile strength (8.13 MPa) indicating superior load-bearing capacity under tension.
- The Fig. 7(b) shows the flexural stress-strain curve where ETI again shows the highest flexural strength (3.2 MPa), making it a suitable choice for bending applications.
- The Fig. 7(c) shows the compression stress-strain curve, with ETI indicating the highest compressive strength

Table 1. Boundary condition for numerical simulation

Aspect	Details (ANSYS-Specific)
Initial Conditions	The composite material is assumed to be in a stress-free state before loading. - Material properties (e.g. Young's modulus, Poisson's ratio, density) are predefined based on experimental data. - No pre-existing deformations or residual stresses are considered. - The model is initialized with room temperature conditions (25 °C) unless thermal effects are studied.
Boundary Conditions - Tensile Test	One end fully constrained (Displacement = 0 in all directions: UX, UY, UZ). - Uniform tensile load applied on the opposite end using a force boundary condition (N) or pressure (MPa). - The load is applied in incremental steps to ensure numerical stability and avoid convergence problems. - Symmetry conditions (UX = 0, UY = 0) are applied for minimizing computational complexity if needed.
Boundary Conditions - Flexural Test	A three-point bending setup was modeled. - Two lower supports fixed (Displacement = 0 in all directions) at equal distances from the center. - A central downward force is applied at the midpoint of the composite specimen. - Contact elements (CONTA174, TARGE170) are used between supports and specimen to simulate realistic loading.
Boundary Conditions - Compression Test	One surface is fully constrained (UX = 0, UY = 0, UZ = 0) to act as a fixed support. - A compressive force (Fz < 0 or Pz < 0) is applied uniformly on the opposite surface. - Frictional contact is defined between compression plates and the composite material to account for realistic constraints. - Buckling analysis is included to assess instability under high compression loads.
Loading Conditions	Loads are applied as force (N) or pressure (MPa) based on experimental results. - Static structural analysis is conducted for mechanical properties evaluation. - For fatigue analysis, cyclic loading is simulated with appropriate amplitude and frequency (e.g., sinusoidal loading with 10^6 cycles). - Dynamic explicit analysis is performed for impact conditions, if applicable.
Meshing & Convergence	A structured mesh with hexahedral elements (SOLID186) is used for improved accuracy. - Mesh refinement strategy: h-adaptive meshing was implemented, with element size determined from sensitivity analysis. - Convergence criteria: Solution convergence is attained when the force and displacement errors are below 1% tolerance. - Element aspect ratio is kept between 1 and 5 to minimize numerical errors.
Solver and Simulation Environment	Simulations are done in ANSYS Workbench/ANSYS Mechanical APDL using Newton-Raphson nonlinear solver. - Nonlinear material behavior (e.g., plasticity, viscoelasticity) is considered if needed. - Contact modeling is implemented using penalty method or augmented Lagrange method. - Large deformation effects are included in flexural and compression tests to capture material failure mechanisms.

Table 2. Mechanical properties of EMC, ETI, ETC, EIS

Bio composite material	Tensile strength (MPa)	Flexural load (KN)	Compression load (KN)	Hardness shore D°
EMC -*Morinda citrifolia*	5.78	0.15	1.92	46
ETI -*Tamarindus indica*	8.13	0.32	5.98	51
ETC-*Tinospora cordifolia*	1.23	0.13	4.11	59
EIS - *Ipomoea staphylina*	2.78	0.19	1.32	45

(5.98 MPa). So, it can withstand significant compressive forces.

- ETC has the minimal tensile and flexural strength, showing weak performance in tension and bending purposes.
- EIS performs moderately among all tests but has lower compressive strength, making it less suitable for structural usages.
- The steeper the curve, the stiffer the material. ETI has the steepest slopes confirming its rigidity.
- EMC exhibits decent tensile and flexural properties but is not as strong as ETI under compression.
- The absence of curves beyond a certain strain value suggests that these materials undergo brittle failure rather than plastic deformation.

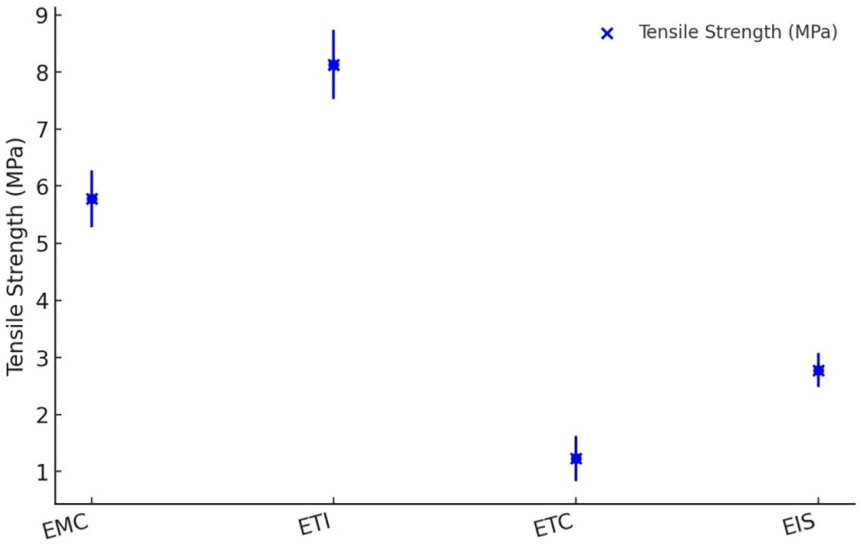

Fig. 3. Variation of tensile strength in different materials

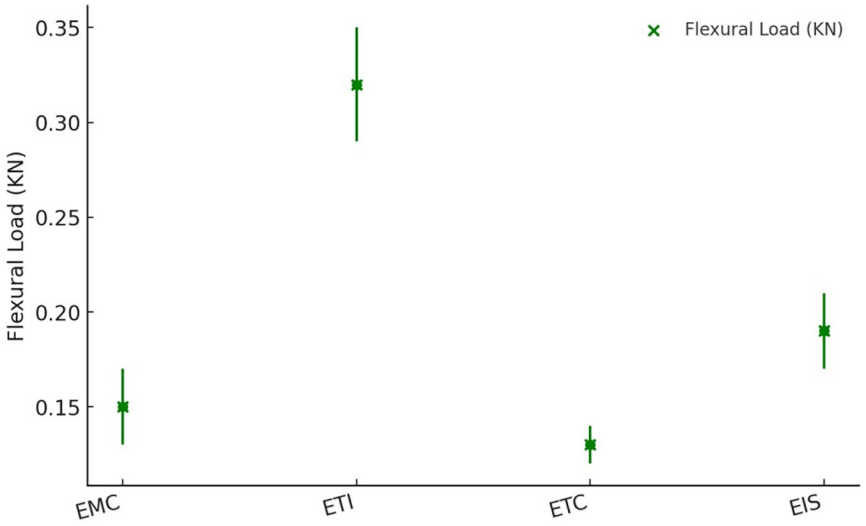

Fig. 4. Variation of flexural load in different materials

Overall, ETI is the best-performing material across all mechanical tests, making it ideal for load-bearing applications in UAV structures.

3.2. FTIR spectral analysis of bio composite

Fibre/matrix bonding was verified using FTIR (Fourier Transform Infrared) spectroscopy; Fig. 8 displays the FTIR analysis of the different bio fibres. The stretching vibrations are recorded in the Tamarindus Indica at a wavenumber of 1637.27 and 1039.44 cm^{-1} due to absorption bands of different substances in schlerenchyma structure. Similar vibrations were detected in *Morinda citrifolia* at 1642.09 and 1031.73 cm^{-1}. Stretching signals were detected in *Tamarindus indica* at 3346.85 and 2915.84 cm^{-1}, which correspond to the hydroxyl groups and C–H bond of the fibre, respectively and in *Morinda citrifolia* at 3341.07 and 2928.38 cm^{-1}, which correspond to the hydroxyl groups and C–H bond of the fibre, respectively [5]. Absorption bands of distinctive groups found in sclerenchyma structure including cellulose, hemicellulose, and lignin in Tinospora Cordifolia, are seen in stretching vibrations detected at wavenumbers of 1636.3 and 1023.05 cm^{-1}. Similar stretching vibrations were detected in *Ipomoea staphylina* at 1633.41 & 1020.16 cm^{-1}. In Tinospora Cordifolia, a stretching hormonic signal is identified at 3299.61 and 2922.59 cm^{-1}, which corresponds to the hydroxyl communities and C–H bond, respectively. Stretching vibrations were detected in *Ipomoea staphylina* at 3327.57 & 2927.41 cm^{-1}, which correspond to the groups of hydroxyl and C–H bonds, respectively, of the fibre.

The FTIR analysis reveals the infrared absorption characteristics of various natural fibre composites: *Tamarindus indica* (blue), *Morinda citrifolia* (red), *Ipomoea*

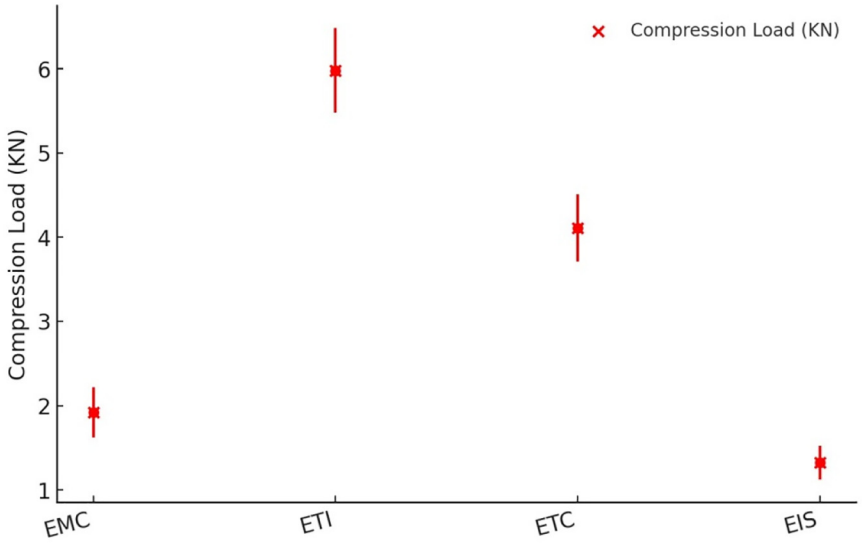

Fig. 5. Variation of compression load in different materials

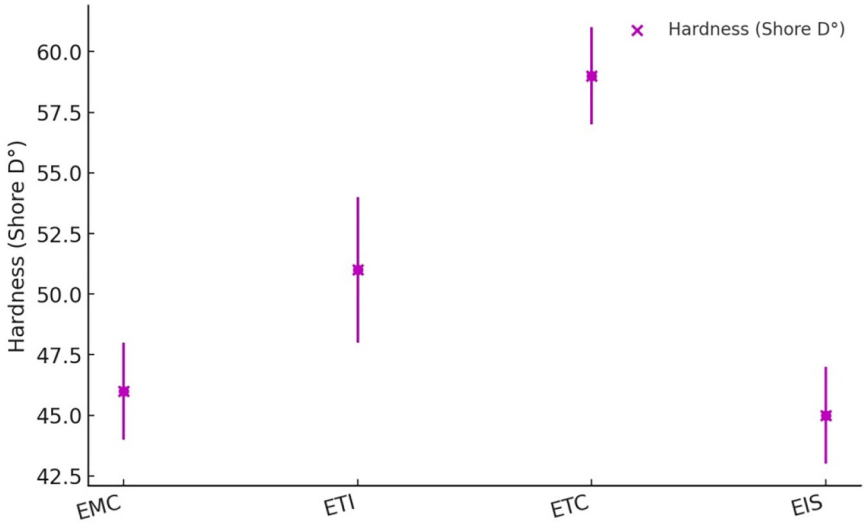

Fig. 6. Variation of hardness in different materials

Table 3. Mechanical properties of natural fibre composites

Sample ID	Tensile strength (MPa)	Tensile strength (MPa)	Compressive strength (MPa)
EMC - *Morinda citrifolia*	5.78	15	1.92
ETI - *Tamarindus indica*	8.13	32	5.98
ETC - *Tinospora cordifolia*	1.23	13	4.11
EIS - *Ipomoea staphylina*	2.78	19	1.32

staphylina (green) and *Tinospora cordifolia* (purple). Each curve displays broad absorption bands in the range of 3,200–3,600 cm^{-1} related to O–H stretching vibrations showing of hydroxyl categories found in cellulose and hemi-cellulose. Around 2,900 cm^{-1}, all samples exhibit peaks due to C–H stretching vibrations from aliphatic groups. The fingerprint region (500–1,500 cm^{-1}) shows a variety of peaks particularly strong around 1,030–1,150 cm^{-1} due to C–O stretching vibrations typical of cellulose and hemicellulose and around 1,315–1,375 cm^{-1}, indicating C–H bending vibrations. Distinct absorption bands near 1,740 cm^{-1} are present in Morinda and Ipomoea spectra attributed to C=O stretching vibrations suggesting acetyl or ester groups. Additional notable peaks include those around 1,500–1,600 cm^{-1} for aromatic ring vibrations from lignin

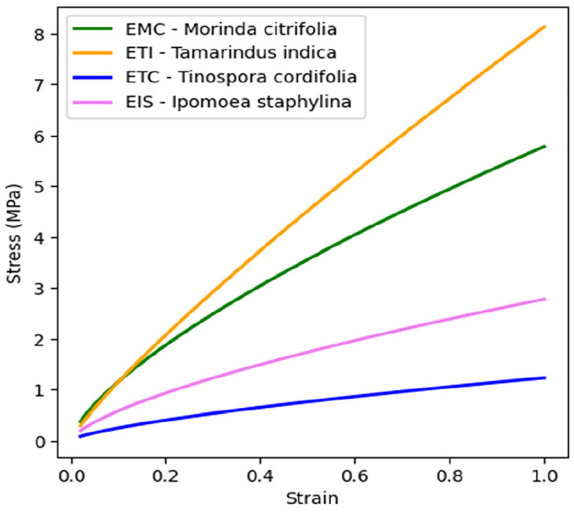

Stress-strain curve of natural composite material in tensile loading
(a)

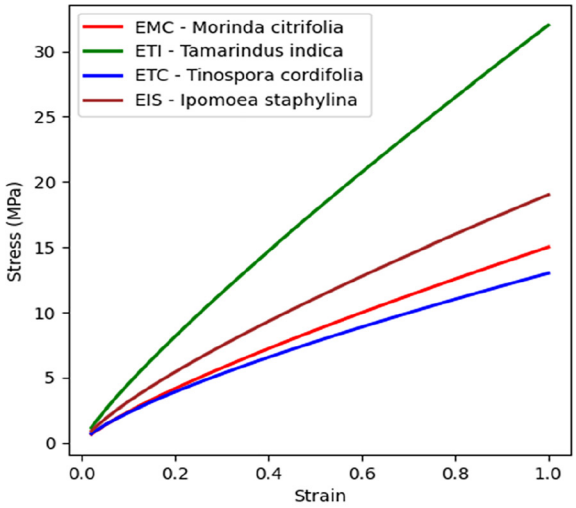

Stress-strain curve of natural composite material in flexural loading
(b)

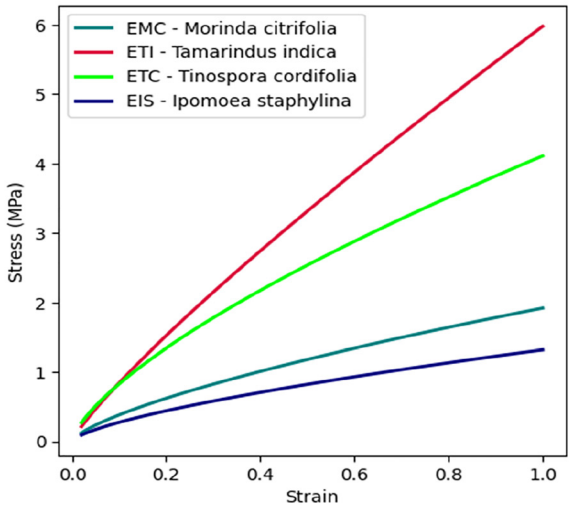

Stress-strain curve of natural composite material in compression loading
(c)

Fig. 7. (a)–(c) Stress strain relationship for various loading condition

and around 1,235 cm^{-1} for C–O–C stretching vibrations linked to ether linkages in lignin. Specifically, *Tamarindus indica* shows unique patterns in the fingerprint region, *Morinda citrifolia* exhibits distinct peaks around 1,740 cm^{-1} indicating higher acetyl or ester content, *Ipomoea staphylina* displays prominent O–H and C=O stretching, and *Tinospora cordifolia* has a smoother spectrum with less pronounced fingerprint region peaks, suggesting different structural compositions. These spectra provide valuable insights into the functional groups and chemical bonds in the fibres, crucial for understanding their mechanical behaviours and potential applications in bio composites.

3.3. Morphological analysis of bio composite

Figure 9 reveals the micro structural analysis of different bio composite structures. It is possible to observe impurities on fibre plate surfaces as well as the presence of parenchyma cells. Figure 9(a) shows a SEM image of *Morinda citrifolia* bio-composites containing impurities as an extra layer on the surface. Figure 9(b) indicates a tamarindus–indica bio composite, where the usage of coupling agent decreases the fibre gathering and increased pull out behaviour. Figure 9(c) represents *Tinospora cordifolia* bio composite, indicating the strong bonding between the fibre-matrix with excellent load-sharing capabilities. Figure 9(d) shows the ipomoea

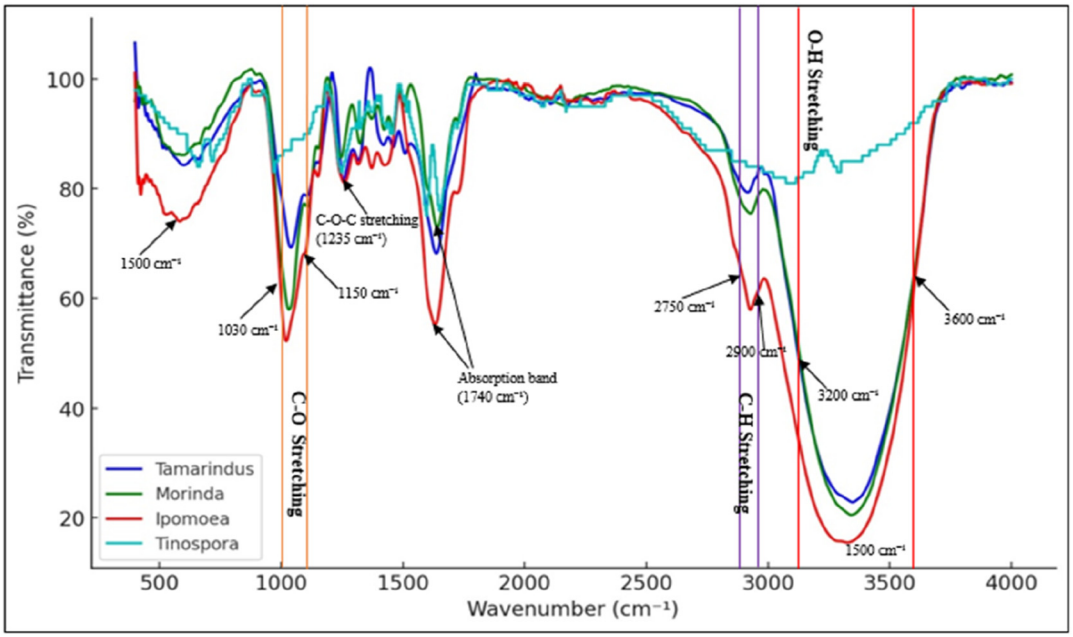

Fig. 8. FT-IR spectra of the samples

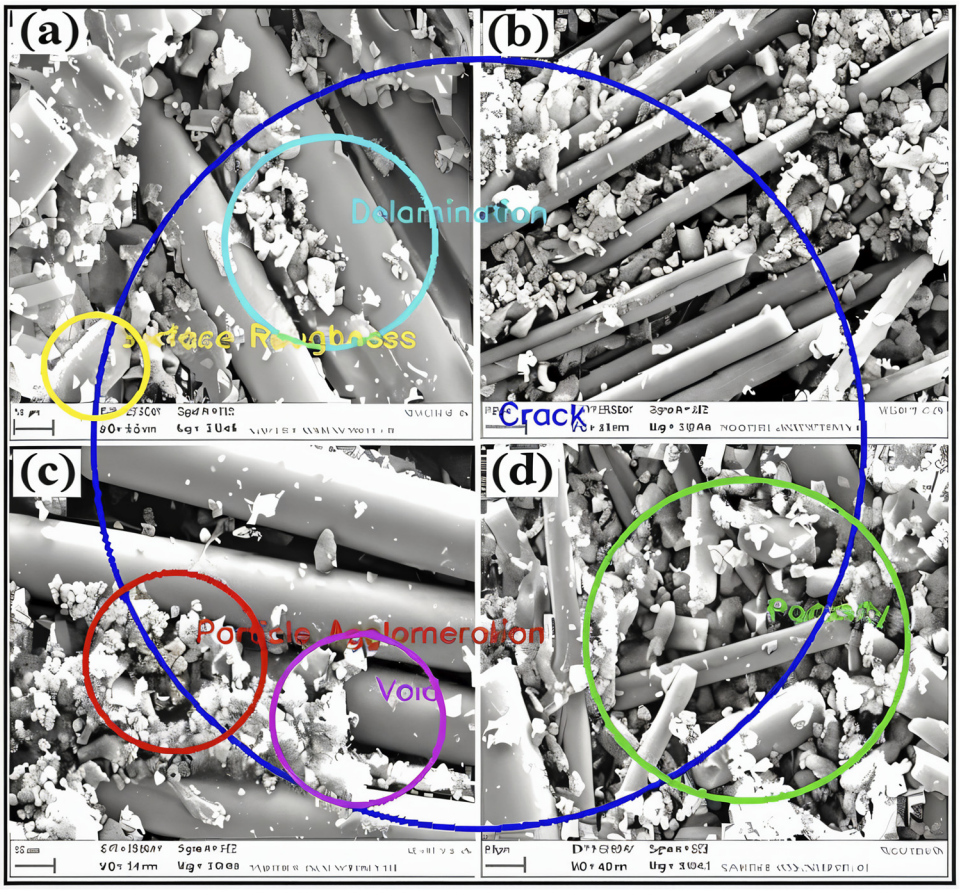

Fig. 9. (a) Sample of epoxy Morinda-citrifolia bio composite, (b) Sample of epoxy Tamarindus–indica bio composite, (c) Sample of epoxy *Tinospora cordifolia* bio composite and (d) Sample of epoxy Ipomoeastaphylina bio composite

staphylina bio composites, depicting residual resin debris on bio fibres and showing the strong bonding with the epoxy.

The Scanning Electron Microscope (SEM) images illustrate the surface morphology of various epoxy-based natural

fibre composites, revealing details about the distribution, bonding and surface characteristics of the fibres within the epoxy matrix. The Epoxy Morinda Citrifolia Composite (EMC) shows smooth and cylindrical *Morinda citrifolia* fibres with some particles and debris on the surface indicating potential weak fibre-matrix bonding areas. The dense network of *Tamarindus indica* fibres in the Epoxy Tamarindus Indica Composite (ETI) exhibits surface roughness and occasional spaces indicating possible weak interfacial bonding locations but acceptable mechanical interlocking. Smooth *Tinospora cordifolia* fibres are uniformly spread over the resin and form Tinospora Cordifolia Composite (ETC), while surface particle matter suggests insufficient wetting or bonding. In locations where interfacial bonding is weak and mechanical integrity may be compromised the Epoxy Ipomoea Staphylina Composite (EIS) exhibits an uneven fibre network with visible holes and gaps surrounding some *Ipomoea staphylina* fibres. Overall, the SEM pictures shed important light on the microstructural features of these composites highlighting the necessity of sufficient fibre-matrix bonding and good fibre dispersion for the best mechanical qualities. The presence of cavities, gaps and particle matter indicates potential locations where the production process should be improved upon to increase the performance of composites.

3.4. Numerical investigation of natural fibre composite panel

For the numerical analysis only ETI and EMC were considered, ETC and EIS were neglected due to their much lower mechanical property values in the experimental work. Figure 10 depicts the distribution of shear elastic strain (XY element) for a composite material subjected to varying compressive loads, specifically 3000, 4000 and 5000 N. In the overall coordinate system, each graphic displays the distribution of strain in millimetres per millimetre across the upper and bottom surfaces of the material at a given time point (1 s). The shear elastic strain for the 3000 N load (03:13 PM) is between −0.00028071 mm mm^{-1} (blue) and 0.00028071 mm mm^{-1} (red). The green colour indicates that the core region is essentially intact, while greater stress concentrations are seen at the corners, showing severe deformation in these places. The strain levels vary from −0.00037428 mm mm^{-1} to 0.00037428 mm mm^{-1} under the 4000 N load (03:11 PM). The core region still shows minor strain, but the additional load causes larger strain values and more noticeable deformation at the corners. The strain distribution for the 5000 N load (03:10 PM) is −0.00046785 to 0.00046785 mm mm^{-1}. The strain values climb as the load is increased further, suggesting increasing deformation and stress concentrations near the margins of the material.

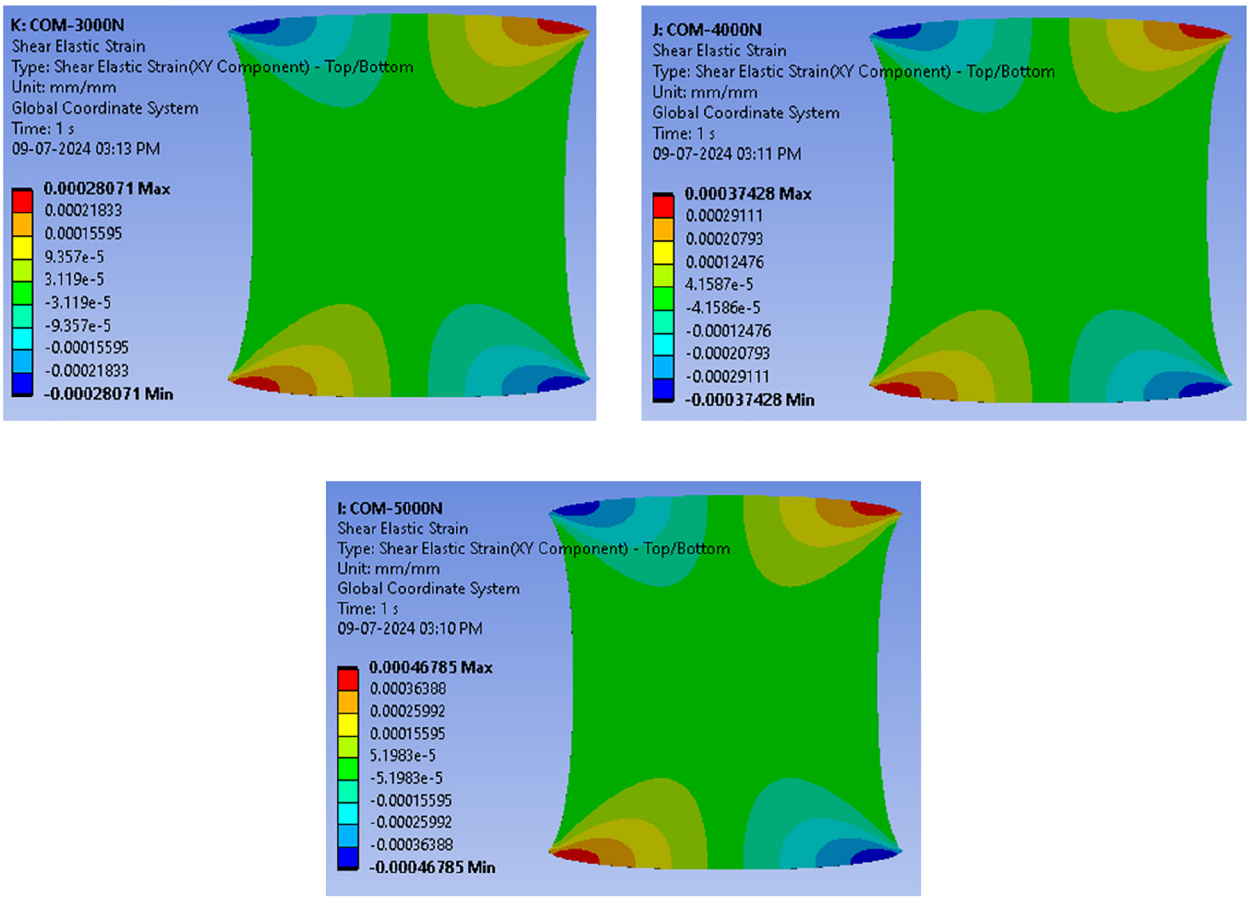

Fig. 10. Variation of shear elastic strain in compression load

All things considered, these contour plots show a very evident trend: when the compressive load rises, so do the highest and lowest shear elastic strain values, leading to increased deformation, especially at the material's corners. The material's edges are especially susceptible to deformation during compressive pressures, as evidenced by the core region's relative stability under low strain. Comprehending the strain distributions is essential for forecasting the behaviour of materials under stress, pinpointing possible locations of failure and refining material design to enhance longevity and efficacy in compressive force-affected applications.

The above Fig. 11 shows the strain energy variation of the composite material with different compressive loads of 3000, 4000, 5000 and 6000 N. At 3000 N the strain energy varies between $8.7684e^{-6}$ and 0.010487 mJ. The middle region exhibits the highest energy signifying substantial deformation. The strain energy range expands from $1.5588e^{-5}$ to 0.018644 mJ when the load increases to 4000 N. A larger red area in the centre indicates improved energy storage because of higher deformation. The strain energy range is further increased in the 5000 N load plot, from $2.4357e^{-5}$ to 0.02913 mJ, with the outlying regions displaying elevated energy levels and the middle region storing even more energy. In conclusion, the strain energy under a 6000 N load varies from $3.5074e^{-5}$ to 0.041949 mJ. The core region shows significant deformation and storage of energy, while the edges and corners also show higher energy levels than under lower pressures. These plots show that the material's strain energy increases with increasing compressive load, especially in the centre region, which is where compressive stress has the greatest impact. Comprehending the strain energy distributions is essential for forecasting the behaviour of materials under stress, pinpointing possible locations of failure, and refining material design to enhance the resilience and efficacy of composite materials in compressive force applications.

For a composite material, Fig. 12 shows the shear stress distribution under different compressive loads: 3000, 4000, 5000, 6000 and 7000 N. In the overall coordinate system, each graphic displays the distribution of shear stresses in MPa across the upper and bottom surfaces of the material at a given time point (1 s). The shear stress for the 3000 N load is −1.0796 MPa (blue) to 0.8399 MPa (red). The core portion, as seen by the green colour is essentially intact, but higher stress intensities are seen around the corners suggesting severe deformation in these places. The stress levels vary between −1.4195 and 1.1176 MPa under the 4000 N load. The core region still shows minor stress but the additional load causes greater stress levels and more noticeable deformation around the corners. The shear stress variation for the 5000 N load is −1.7994–1.3994 MPa. The stress values grow in response to

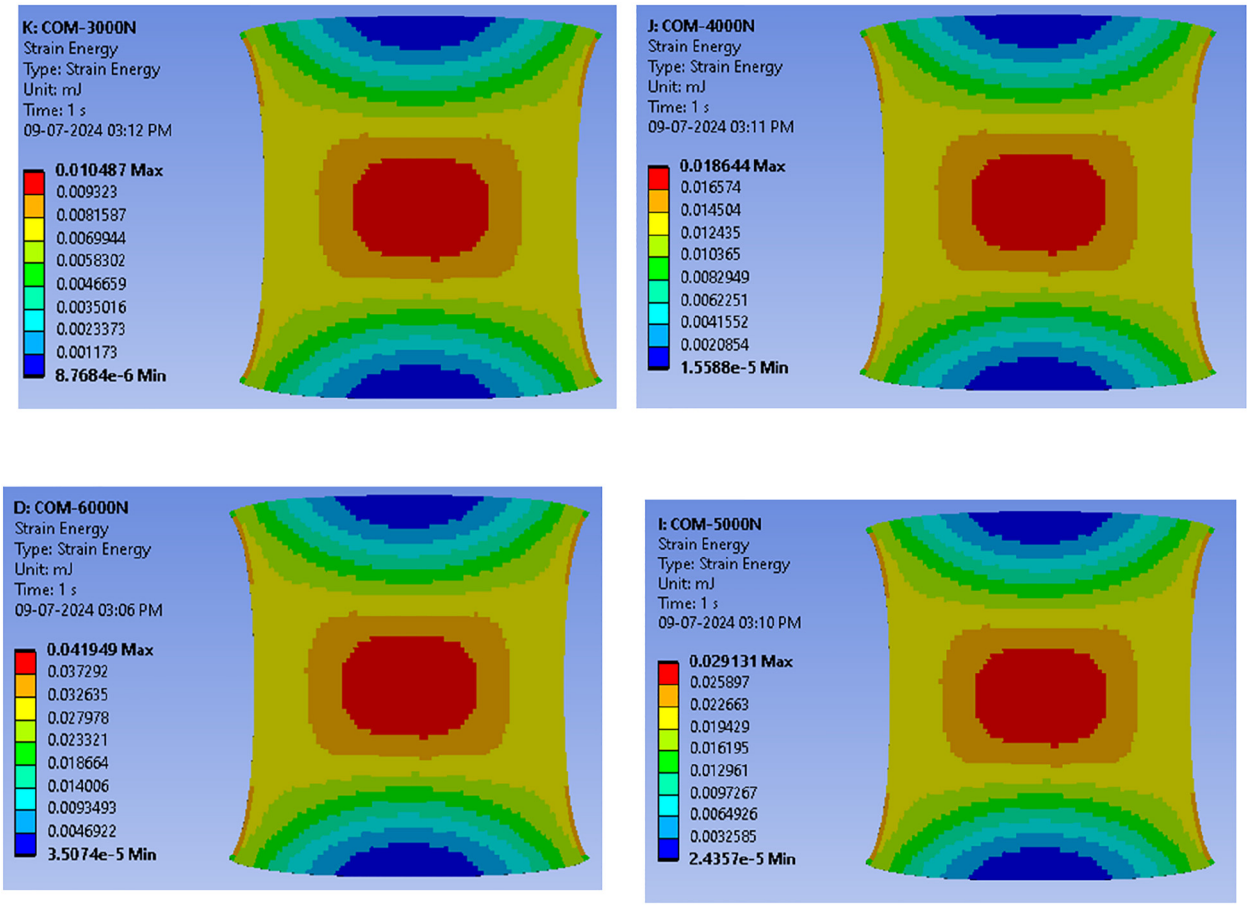

Fig. 11. Variation of strain energy in compression load

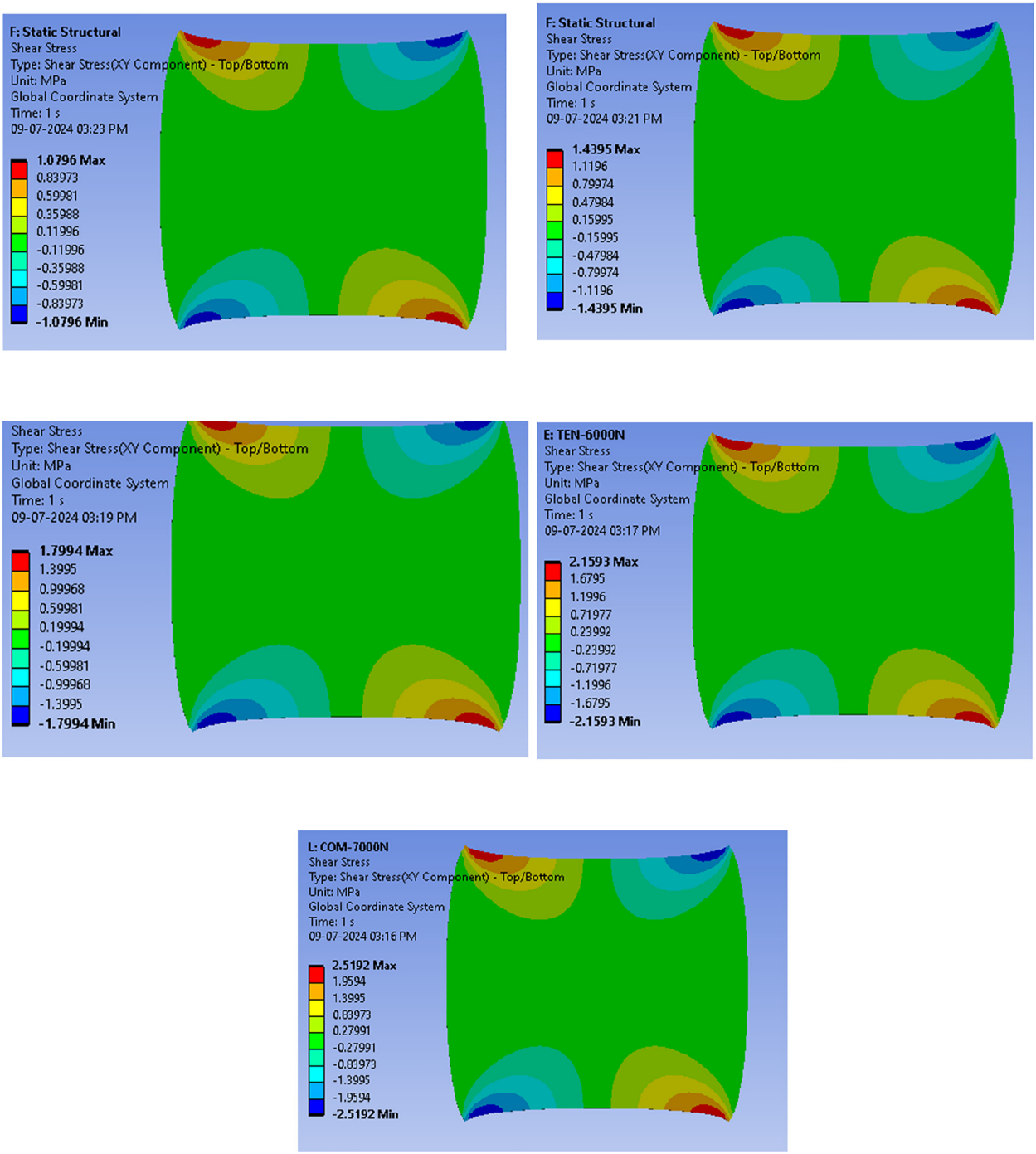

Fig. 12. Variation of shear stress in tensile load

the additional load, suggesting increasing deformation and stress concentrations near the margins of the material. The stress varies from −2.1595 to 1.7995 MPa at 6000 N. Shear stress in the core region rises and the deformation structure becomes more obvious, especially around the edges and corners. Lastly, the shear stress varies between −2.5192 and 2.1592 MPa for the 7000 N load. The material experiences considerable deformation and stress concentrations at the corners and edges under this load resulting in the greatest stress values. All things considered, these contour plots show a very evident trend: when the compressive load rises, so do the maximum and lowest shear stress values, which leads to more substantial deformation, especially at the material's corners. The material's edges are highly susceptible to deformation during compressive pressures as evidenced by the central region's relative stability under low stress. Comprehending the stress distributions is essential for forecasting the behaviour of materials under stress, pinpointing possible locations of failure, and refining material design to enhance longevity and efficacy in compressive force applications.

Figure 13 shows the total deformation (mm) of *Tamarindus indica* and *Morinda citrifolia* with various compressive loads (N). The *Tamarindus indica* indicates a minimum deformation of 0.016 mm up to 6000 N compressive loads. From this, *Tamarindus indica* possesses maximum resistance to deformation due to inner structural integrity. But *Morinda citrifolia* shows the highest deformation of 0.032 mm at 6000 N compressive loads due to its lower resistance against the compressive stresses. From this result, it is clear that *Tamarindus indica* is more rigid and stiffer to maintain its shape under load, but *Morinda citrifolia* possesses more dampening and flexible properties due to its deformation.

The relationship between directional deformation (in mm) and compressive load (in N) for two composite materials, *Tamarindus indica* and *Morinda citrifolia* is shown in Fig. 14. These two materials behave differently mechanically when subjected to compressive force. The light blue line, *Tamarindus indica*, shows very little directional deformation

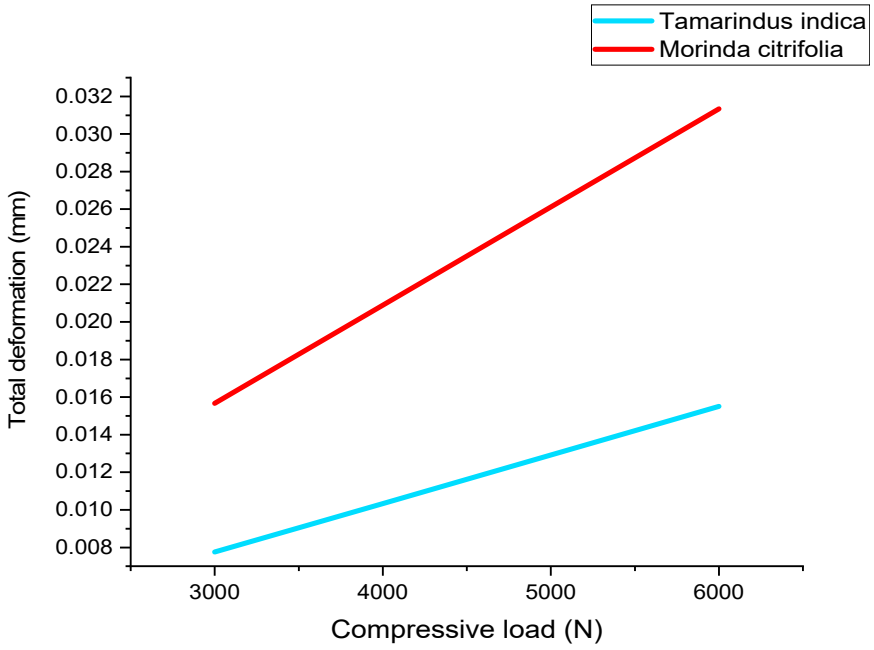

Fig. 13. Variation of total deformation in compression load

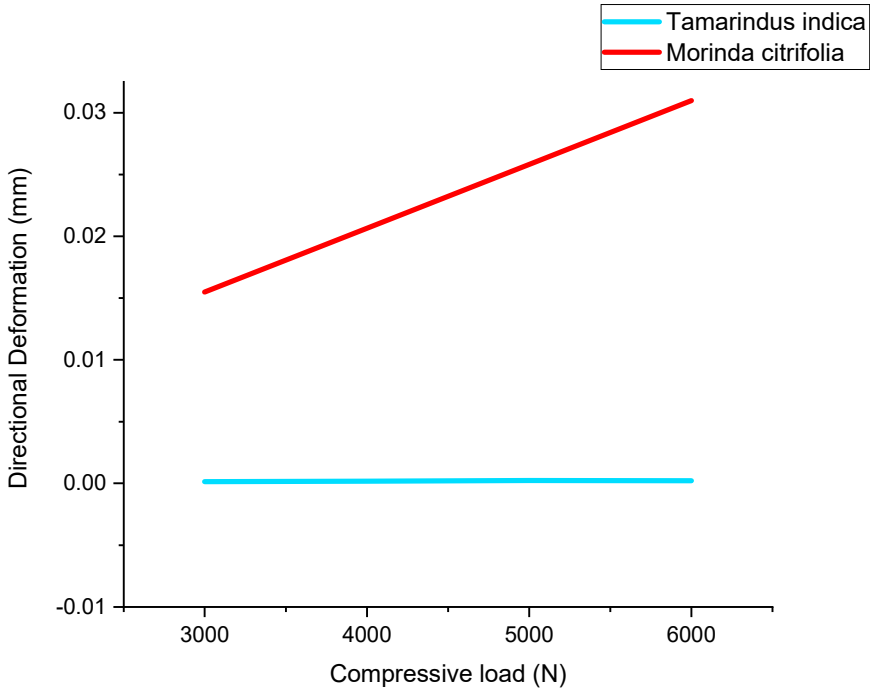

Fig. 14. Variation of directional deformation in compression load

as compressive loads increase. *Tamarindus indica* provides strong resistance to compressive deformation from the load of 3000 to 6000 N. Due to this behaviour, *Tamarindus indica* gives better structural integrity and stiffness in the compressive load. So, the *Tamarindus indica* is the optimum material for construction applications to protect the shape and rigidity under the compressive load. In other cases, *Morinda citrifolia* exhibits an elevated directional deformation against the compressive force. The deformation varies from 0.01 to 0.03 mm according to load variation from 3000 to 6000 N because of its internal molecular bonding and composition. So, the Morinda citrifolias can be used in isolating applications where the flexibility is more dominant.

Figure 15 indicates the equivalent elastic strain variation of *Tamarindus indica* and *Morinda citrifolia* with different compressive loads from 3000 to 6000 N. *Tamarindus indica* indicates a strong, consistent elastic behaviour and decreased deformability with a linear rise in strain from 0.00010 at 3000 N to 0.00015 at 6000 N. In the case of *Morinda citrifolia*, it possesses the higher strain approximately from 0.00025 at 3000 N to 0.00045 at 6000 N, and it shows Morinda possesses high deformation and sensitiveness against the load variation. As well as *Tamarindus indica*, they possess less strain and low sensitivity against the load.

Figure 16 shows the strain energy variation against the compressive load for *Tamarindus indica* & *Morinda citrifolia*. The strain energy for *Tamarindus indica* rises uniformly from about 0.005 mJ at 3000 N to about 0.015 mJ at 6000 N, representing a steady and medium capacity for energy absorption. In another case, the strain energy of *Morinda citrifolia* rises at a faster rate from 0.015 mJ at 3000 N to 0.040 mJ at 6000 N. This gives that comparison to *Tamarindus indica*; *Morinda citrifolia* has a greater capability for energy absorption against the compressive stresses. *Morinda citrifolia* seems to be better in energy absorption so that it can be used in damping applications to absorb the vibration energy.

Plotted against the location along the x-axis, Fig. 17 displays the total deformation, measured in millimeters (mm), of *Tamarindus indica* during various tensile strains. The four tensile loads are shown as follows: 6000 N (orange line), 5000 N (green line), 4000 N (cyan line) and 3000 N (purple line). Along the position, the deformation increases linearly with the tensile load. The distortion begins at 0 mm and increases progressively to around 0.01 mm in the longest place during a 3000 N load. Similar trends are shown with the 4000 N load, although there is more deformation up to 0.015 mm. Even greater deformation is brought up by the 5000 N load, which peaks at about 0.02 mm. The maximum deformation, which culminates at approximately 0.03 mm, is caused by the 6000 N load. The material consistently stretches over its length when applied tensile loads are applied, as indicated by the linear relationship between position and deformation. This illustrates the elastic behaviour of the material and its ability to deform under a range of tensile stresses: the larger the applied load, the higher the total deformation. Grasping *Tamarindus indica*'s mechanical qualities and applicability for applications needing particular deformation characteristics during tensile loading requires a grasp of this information.

The distribution of shear stress under various tensile loads that vary from 3000 to 7000 N is shown in Fig. 18 throughout the entire length of *Tamarindus indica*. Tensile loads are represented by the following coloured lines: 7000 N (brown), 5000 N (yellow), 6000 N (red), 4000 N (cyan) and 3000 N (purple). Every line, which crosses the y-axis at zero

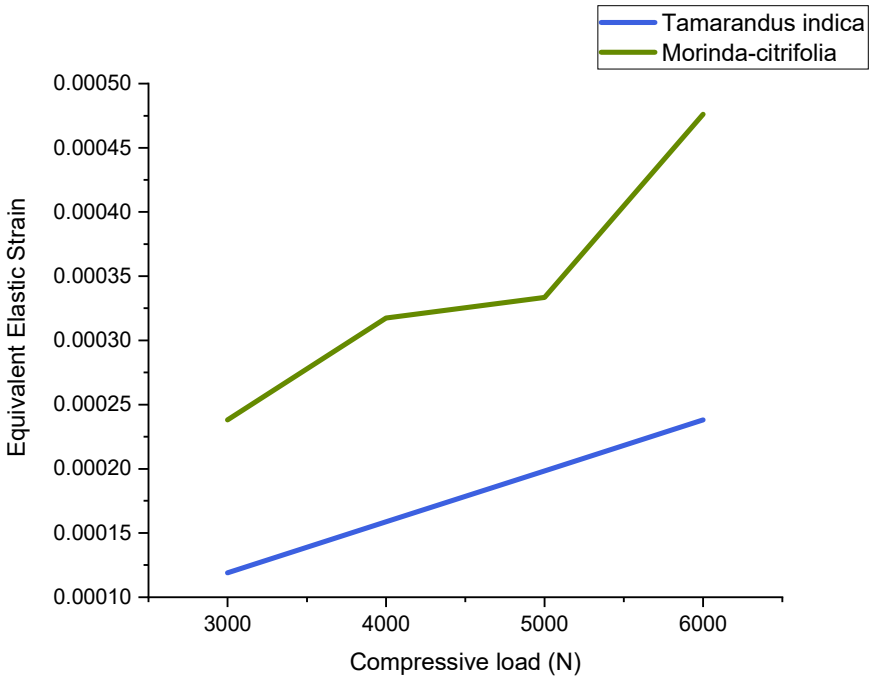

Fig. 15. Variation of equivalent elastic strain in compression load

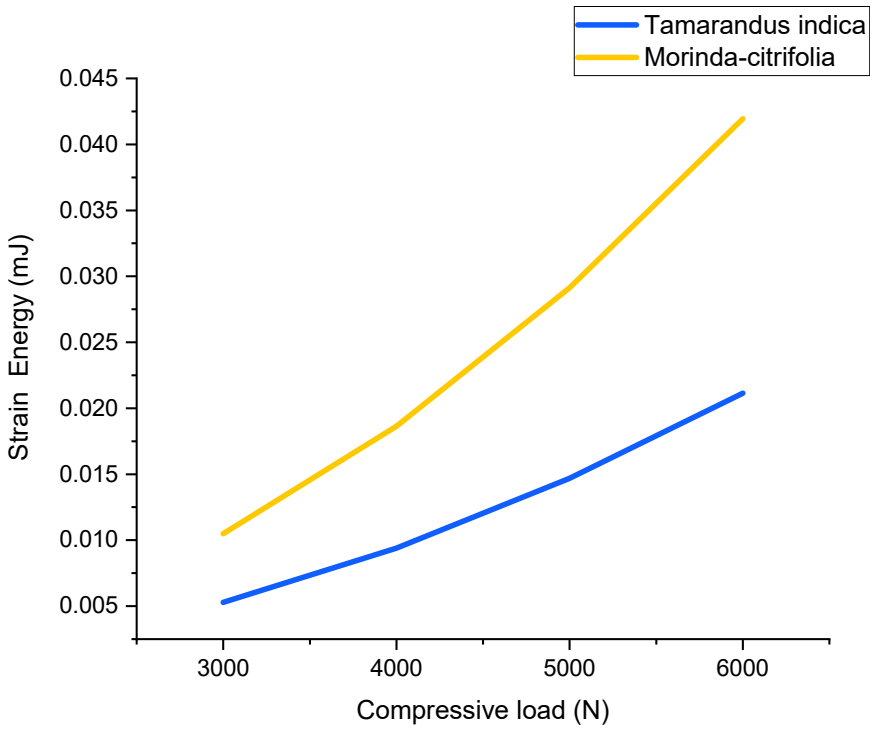

Fig. 16. Variation of strain energy in compression load

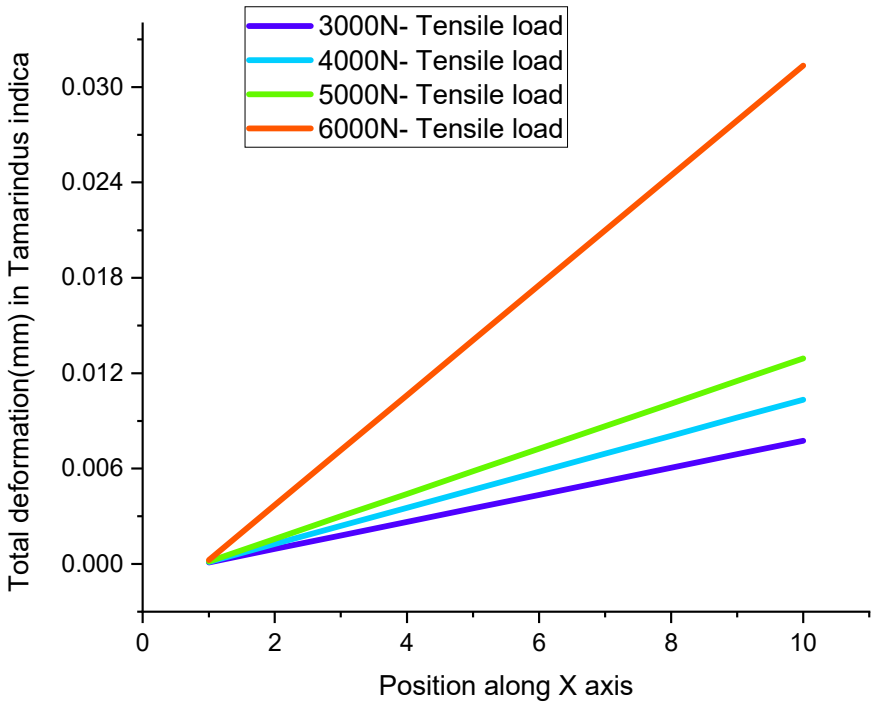

Fig. 17. Variation of total deformation along the x direction

and extends symmetrically in both positive and negative directions, depicts the linear connection among the position throughout the length and the shear stress. The slope of the lines suddenly increases with respect to tensile load remarking a higher value of shear stress. For example, the shear stress varies between −1.5 and 1.5 MPa at a 3000 N load and −2.5 and 2.5 MPa at a 7000 N load. At tensile load application, the material may attain homogeneous shear stress along the length, according to this uniform and symmetric distribution.

Figure 19 indicates the variation of total deformation with different tensile loads ranging from 2000 to 7000 N.

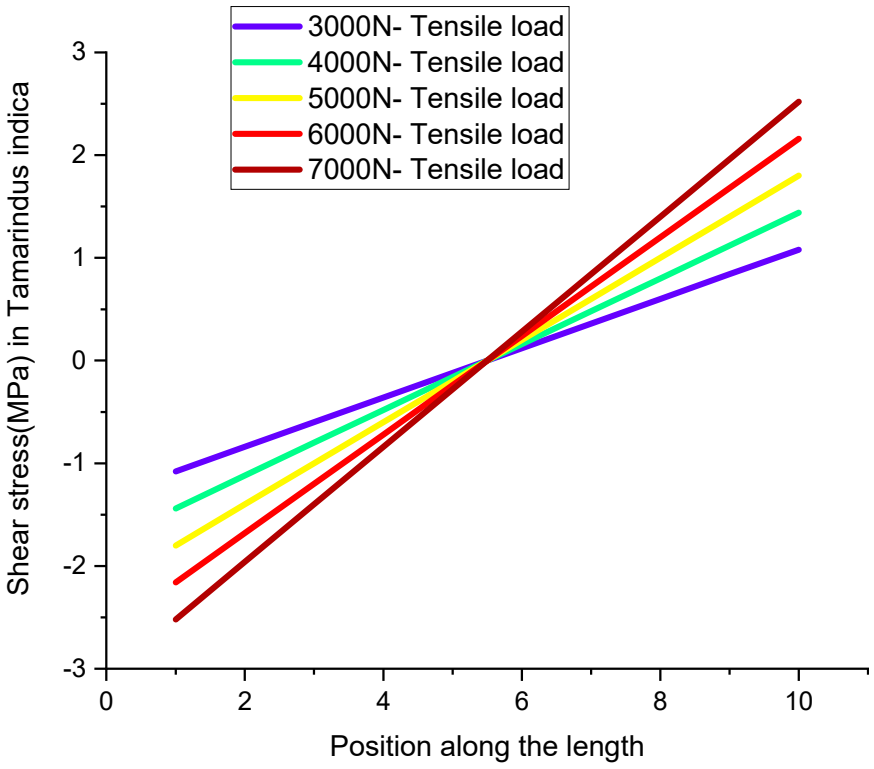

Fig. 18. Variation of shear stress along x direction

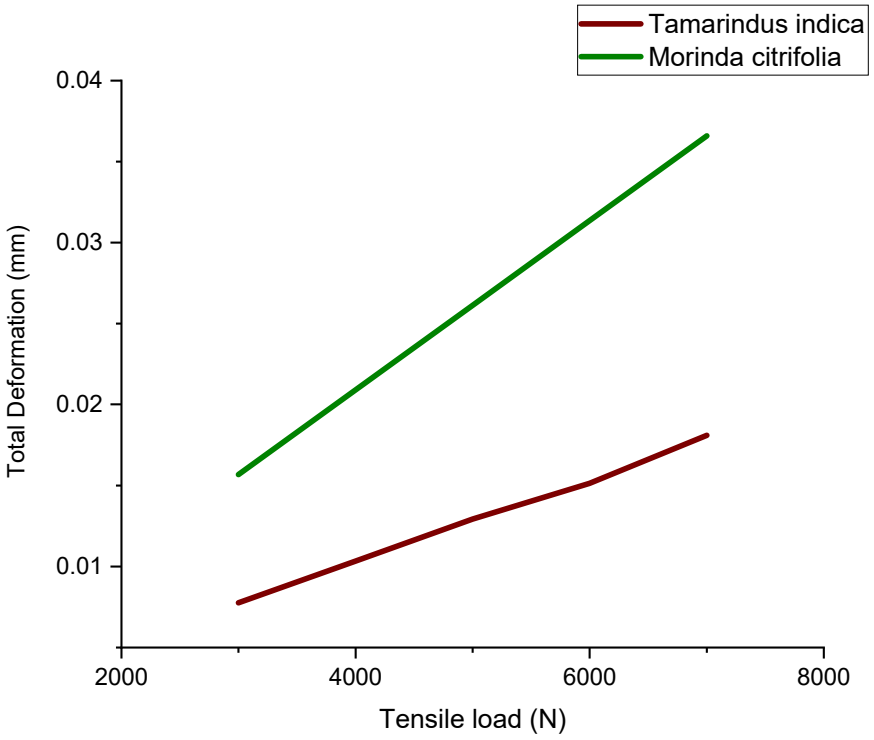

Fig. 19. Comparison of total deformation among the natural fibres

While the total deformation of two materials rises with an increase in the tensile load, *Morinda citrifolia* shows higher deformation at all stress values than *Tamarindus indica*. For example, at 7000 N *Tamarindus indica* barely deforms about 0.015 mm but *Morinda citrifolia* attains a deformation of about 0.035 mm. This suggests that *Morinda citrifolia* is less stiff or more elastic than *Tamarindus indica*, as it is more prone to deformation during tensile stress.

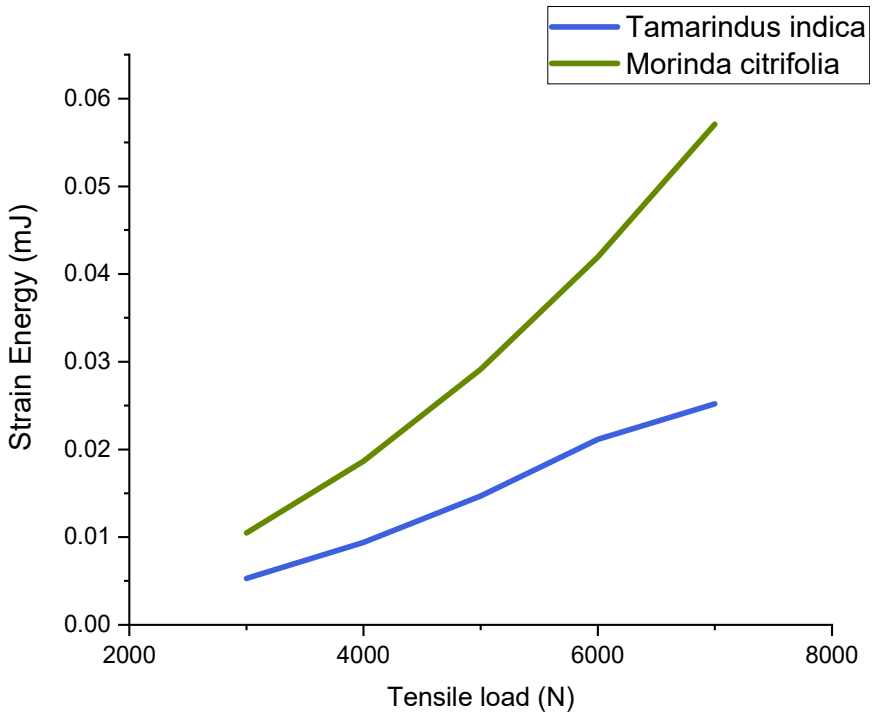

Fig. 20. Comparison of strain energy among the natural fibres

Although the deformation rise for both materials is linear, indicating consistent elastic behaviour the differing slopes emphasize the unique mechanical features of each material. *Tamarindus indica* would be preferred in scenarios requiring reduced deformation, while *Morinda citrifolia* could be appropriate for applications where increased flexibility and deformation are favourable. This contrast is important for applications requiring certain deformation properties.

Tamarindus indica and *Morinda citrifolia* are the two materials whose strain energies (mJ) are shown in Fig. 20 under a range of tensile loads, from 2000 to 7000 N. When tensile loads increase, both materials show a rise in strain energy; however, *Morinda citrifolia* exhibits significantly greater strain energy at every load level than *Tamarindus indica*. For instance, *Tamarindus indica* reaches roughly 0.02 mJ of strain energy at 7000 N, while *Morinda citrifolia* reaches about 0.06 mJ. This suggests that *Morinda citrifolia* is more flexible or less stiff than *Tamarindus indica* because it absorbed more energy under tensile stress. *Tamarindus indica* is good for applications that require a lower absorption of energy, while *Morinda citrifolia* is good for requiring high energy absorption and flexibility applications.

4. CONCLUSION

From the overall investigation the forthcoming bio composite materials such as EMC, ETI, ETC, and EIS, along with a comparison of *Tamarindus indica* and *Morinda citrifolia*, we deliver information about their suitable applications. From the analysis, it is clearly shown that ETI possesses good mechanical characteristics like higher tensile strength (8 MPa), flexural load capability (0.35 kN) and compressive load capability (6 kN). Due to these properties, ETI is a suitable material for more weight-bearing and high-strength applications. In another case, ETC possesses a lesser value of flexural load-carrying capacity (0.1 kN) and tensile strength (2 MPa). Instead of having the highest hardness value of 60 Shore D°, it sustains poorly for all load conditions, showing that it is not suitable for high-stress applications. The comparison of *Tamarindus indica* and *Morinda citrifolia* shows remarkably higher total deformation and equivalent elastic strain at various compression and tension loads. It is clear that *Morinda citrifolia* possesses higher flexibility and lower stiffness than *Tamarindus indica*. The strain energy analysis indicates the *Morinda citrifolia* is capable of high energy absorption by an influence of tensile stress so that it can be used as dampening or cushioning material to absorb the vibrational energy.

4.1. Future research directions

1. Optimization of Fabrication Processes—Enhancing techniques like vacuum-assisted resin transfer melding (VARTM) or hot pressing can improve the mechanical performance and consistency of bio-composites.
2. Chemical Treatments for Better Fibre-Matrix Bonding—Investigating surface treatments (e.g., alkali, silane, plasma) can enhance adhesion, leading to stronger and more durable composites.
3. Environmental Impact and Life Cycle Assessment (LCA)—Evaluating biodegradability, carbon footprint and recyclability will help establish bio composites as truly sustainable alternatives.

4. Hybrid Bio-Composites Development—Combining multiple bio-fibres (e.g., *Morinda citrifolia* with hemp or jute) can optimize mechanical properties like tensile strength and impact resistance.
5. Long-Term Durability and Aging Studies—Testing composites under extreme conditions (UV exposure, humidity, temperature changes) will determine their real-world performance and lifespan.

REFERENCES

[1] H. J. Aida, R. Nadlene, M. T. Mastura, L. Yusriah, D. Sivakumar, and R. A. Ilyas, "Natural fibre filament for fused deposition modelling (FDM): a review," *Int. J. Sustain. Eng.*, vol. 14, pp. 1988–2008, 2021.

[2] M. A. Al Faruque, M. Salauddin, M. M. Raihan, I. Z. Chowdhury, F. Ahmed, and S. S. Shimo, "Bast fiber reinforced green polymer composites: a review on their classification, properties, and applications," *J. Nat. Fibers*, vol. 19, pp. 8006–21, 2022.

[3] A. A. Arman Alim, S. S. Mohammad Shirajuddin, and F. H. Anuar, "A review of nonbiodegradable and biodegradable composites for food packaging application," *J. Chem.*, vol. 2022, pp. 1–27, 2022.

[4] H. Awais, Y. Nawab, A. Amjad, A. Anjang, H. Md Akil, and M. S. Zainol Abidin, "Environmental benign natural fibre reinforced thermoplastic composites: a review," *Composites Part c: Open Access*, vol. 4, 2021, Art no. 100082.

[5] J. Berglund, D. Mikkelsen, B. M. Flanagan, S. Dhital, S. Gaunitz, G. Henriksson, M. E. Lindström, G. E. Yakubov, M. J. Gidley, and F. Vilaplana, "Wood hemicelluloses exert distinct biomechanical contributions to cellulose fibrillar networks," *Nat. Commun.*, vol. 11, p. 4692, 2020.

[6] A. Bernaoui, G. Lebrun, and E. Ruiz, "High performance natural fiber composites from mat and UD flax reinforcements backed with a mat binder: a study of mat fiber surface fibrillation," *Compos. Part A. Appl. Sci. Manuf*, vol. 160, 2022, Art no. 107064.

[7] D. Bhardwaj, A. Gupta, V. Chaudhary, and S. Gupta, "Hybridization of natural fibers to develop the polymeric composite materials: a review," in *Advances in Engineering Materials*, 2021, pp. 355–63.

[8] X. Bi and R. Huang, "3D printing of natural fiber and composites: a state-of-the-art review," *Mater. des*, vol. 222, 2022, Art no. 111065.

[9] I. L. Costa, P. H. Pereira, A. M. Claro, N. C. Amaral, H. D. S. Barud, R. B. Ribeiro, and D. R. Mulinari, "3D-printing pen from valorization of pine cone residues as reinforcement in acrylonitrile butadiene styrene (ABS): microstructure and thermal properties," *J. Thermoplast Compos. Mater.*, vol. 36, pp. 535–54, 2023.

[10] M. Vinothkumar, V. Jaiganesh, and R. Raviraja Malarvannan, "Effects of surface-modified pineapple fibre-reinforced micro B4C and CTBN rubber particle toughened epoxy hybrid composites in mechanical, impact damage, thermal and water absorption behavior," *Mater. Res. Express*, vol. 6, no. 11, 2019, Art no. 115343.

[11] V. Jaiganesh, M. Vinothkumar, and P. Gurusamy, "Fatigue, fracture toughness and dynamic mechanical behaviour of CTBN rubber toughened silane surface-modified pineapple fiber and micro B_4C-reinforced epoxy hybrid composites," *Biomass Convers. Biorefinery*, vol. 14, no. 8, pp. 9739–48, 2024.

[12] V. K. Mamidi, R. Pugazhenthi, G. Manikandan, and M. V. Kumar, "Mechanical and microscopic study on Tinospora cordifolia and Tectona grandis composites," *Mater. Today Proc.*, vol. 22, pp. 772–5, 2020.